國立交通大學

電機資訊學院 電子與光電學程

碩 士 論 文

電 子 穿 越 肖 基 障 之 一 致 化 模 擬

A Unified Simulation of ElectronTransmission through the Schottky Barrier

研 究 生：賴韋仲

指導教授：郭雙發　教授

中 華 民 國 九 十 四 年 六 月

電子穿越肖基障之一致化模擬

A Unified Simulation of ElectronTransmission through the Schottky Barrier

學　　生：賴韋仲　　Student : Sierra Lai

指導教授：郭雙發　　Advisor : Prof. Shuang-Fa Guo

國立交通大學

電機資訊在職專班　電子光電組

碩士論文

A Thesis of Master Degree

Institute of degree program of Electrical Engineering and Computer Science

Electronics and Optical Group

National Chiao-Tung University

June, 2005

Hsin-Chu, Taiwan, R.O.C

中華民國九十四年六月

電子穿越肖基障之一致化模擬

學　　生：賴韋仲　　指導教授：郭雙發教授

國立交通大學電機資訊學院 電子與光電學程（研究所）碩士班

摘要

在此論文中我們已經發展一個數值模擬程式來探討電子穿越金屬版導體接面的現象。能障的分布在半導體的表面被適當地分成幾個小區塊，能障位能可近似一連串的線性區塊或階梯狀區塊。藉由 airy function 來解薛晶格方程式可以產生一個轉移矩陣來表示每一小區塊裡的電子傳輸現象。電子穿越整個接面能障的穿越係數可以每一小區塊的轉移矩陣相乘而得，並與傳統的 WKB 近似法所求的穿越係數做比較。

不論電子能量大於或小於接面能障，電子傳輸係數都可以被計算出來，所以我們首次提出電子穿越半導體表面及金屬半導體介面電子熱傳輸之一致化模擬。傳輸係數是金屬至半導體電子移轉機率的方程式，而越過肖基障的熱傳導電流可由經由對傳輸係數的積分而得。而電子穿越肖基障的電流則可以轉成電子電動的合併及產生過程，此一過程與半導體的費米能階與未能分佈有關。這電子穿越過程與半導體中電流的傳輸能自發性前後一致地連結起來。

在不同傳輸模型及不同參雜濃度下的傳輸係數與電子能量的相關性及熱傳導電流與外加偏壓的關係也在此論文中加以討論。

A Unified Simulation of ElectronTransmission through the Schottky Barrier

Student: Wei-Tsung Lai Advisor : Prof. Shuang-Fa Guo

Degree Program of Electrical Engineering Computer Science
National Chiao Tung University

Abstract

A numerical simulation program has been developed in this work to investigate the transmission of electrons through the metal-semiconductor contacts. The semiconductor surface is discretized properly into a number of small intervals and the potential barrier is approximated as a series of piece-wise linear or step functions. The transfer matrix for electron transmission through or cross each interval of simple potential distribution can be obtained by solving the Schrödinger equation using Airy or exponential function. The transmission coefficient of electrons through or across the whole contact barrier is then derived from the cascaded transfer matrices. As a comparison, the conventional WKB approximation method has also been illustrated.

Since the transmission coefficient can be calculated numerically for electron with energy below or above the contact barrier, we propose, for the first time, a unified simulation for electron tunneling through the semiconductor surface and thermionic-emission at the metal-semiconductor interface. The thermionic-emission current across the Schottky barrier is integrated from the transmission coefficient, which is a function of electron energy together with the transition probability of electron between metal and semiconductor. However, the tunneling current through the Schottky barrier is converted into a local generation or recombination process with

local rate depending on the local Fermi-level and the potential distribution. The tunneling processes are self-consistently treated with all current transport in the semiconductor.

The transmission coefficient is a function of electron energy as well as the tunneling and thermionic-emission currents as a function of applied voltage for different transmission models and various doping concentrations has been discussed in this paper.

誌　　謝

During my study of this thesis, I would like to thanks Professor Guo very much. He spent a lot of time and had more pensions on me to do couching and guiding. I can not finish my thesis without him. I do appreciate all of his efforts. Besides, my families, friends and colleagues also encourage and stick on me during the hard time of my work and study. The contribution of this work should belong to all related persons.

圖目錄

符 號 說 明

m^* ：effective mass of electron

$\hbar$ ：reduced Planck constant

y ：wave function

Ai ：Airy function of the first kind

Bi ：complementary Airy function

Γ ：The transmission coefficient

p ：classical momentum

f ：Potential energy

f_m ：Fermi-Dirac distribution functions in the metal

f_s ：Fermi-Dirac distribution functions in the semiconductor

Ω ：atomic volume

x_b ：barrier height

F_{ms} ：Transition probability

Δf ：Schottky barrier lowering

Xm ：Interfacial layer thickness

G ：Local generation rate

Chapter 1 Introduction

For future design of deep sub-micron device, metal-semiconductor contact is an important consideration in the development of integrated circuit technology. It may work as a rectifying Schottky or pure ohmic contact depending on the metal work function and semiconductor impurity concentration. It is important to predict the effect of the Schottky contact on the semiconductor devices by the numerical simulation to promote the circuit development [1]. From the device design point of view, a practical and accurate model for the metal-semiconductor contact should be established.

Numerical approaches should be employed to calculate the electrical characteristic of metal-semiconductor contact under various conditions. The method in which only the thermionic emission at the metal-semiconductor interface is considered is simple and accurate for Schottky barrier diodes at low impurity concentrations or under low bias conditions [2]. However, it is insufficient when the tunneling phenomenon is dominated at high impurity concentration or under reverse bias. The tunneling current has been included as the current boundary condition at the metal-semiconductor interface in addition to the thermionic emission current [3,4]. Naturally, this method is not expected to be accurate when tunneling occurs far from the interface. Under this condition, the distribution of carriers and potential would be inaccurate in self-consistent calculations since all carriers are artificially injected at the interface. The region for calculating the tunneling current has been estimated and the carrier transport by drift and diffusion has been neglected inside the region [5,6]. This ignorance of carrier transport in the tunneling region would cause inaccuracy of potential and carrier distribution in the space charge region due to Schottky barrier.

Recently, Ieong et al [7] have presented a physical contact model where all

tunneling processes are self-consistently treated with all current transport in the semiconductor. The key feature of the model is that tunneling current through the barrier is converted into a spatially distributed generation or recombination process where the local generation rate depends on the local Fermi-level at each grid and the potential profile along the tunneling path. The tunneling integral over distance and energy can be transformed into a double integral over distance alone.

The transmission coefficient of an electron through the Schottky barrier plays a key for the calculation of tunneling current. The Wentzel-Kramers-Brillouin (WKB) approximation has been widely used due to its simple mathematical form [1,7]. However, this approximation is not valid for the potential variation in the contact barrier is not very slowly in the general device structures. The purpose of this work is to present a more accurate numerical method to solve the Schrodinger equation in arbitrary contact potential.

Analytical solutions for Schrodinger equation exist only for some particular potential distributions such as constant potential and constant field [8,9]. Plane wave and evanescent wave solutions can be used for a step potential. The exact solution of a particle in a uniform static field can be expressed as a linear combination of Airy and complementary Airy functions.

The transfer matrix approach introduced by Tsu and Esaki [10] has been used for transmission coefficient calculation. This approach is easily extended to many layer structures with electron energy above or below the potential distribution.

The thermionic emission current can be evaluated with the calculated transmission coefficient. A unified simulation for electron transmission through the Schottky barrier is proposed in this work. The effective barrier lowering has been included in the calculation of thermionic emission current. The tunneling process is self-consistently treated with all current transport in the semiconductor [7].

In Chapter 2, several analytic solutions are introduced for transmission coefficient calculation. Single barrier is used to illuminate the Airy function and exponential function solution and then expressed in Matrix form. The electron energy over and under the barrier potential are also discussed. The traditional WKB approximation method and its limitation is explained for comparison.

In Chapter 3, some numerical simulation techniques which are used in the developed program are introduced. The space discretization concept is important for tunneling current calculation of Schottky barrier. The barrier is divided into n sections for the tunneling current calculation at each grid by transfer matrix formulation. The current density through the Schottky barrier includes the thermoinic-emission at the interface and tunneling current at bulk region. A self-consistent calculation is introduced to well link the tunneling process and thermoinic-emission process with all current transport through the Schottky barrier. The key to calculate the tunneling current through the barrier is converted into a local generation rate or recombination process which can be got by solving the device equations with boundary conditions. The barrier lowering effect is also considered with a voltage drop at the interfacial layer. The thickness of interfacial layer can be calculated for electric field calculation. The key contribution in this paper is the unified simulation for thermionic emission current calculation since the transmission coefficient can be calculated for the electron energy above the Schottky barrier.

In Chapter 4, all the simulation results and discussion are presented. They break into several parts in term of transmission coefficient of different transmission models, transition probability of different degeneracy models, generation rate as a function of electric field, transmission coefficient and transition probability, and unified simulation for current density through the Schottky barrier.

In Chapter 5, our conclusions are shown.

Chapter 2 Transmission Models

2.1 Analytic Solutions of Schrödinger Equation

The transmission of electrons through a potential barrier is usually investigated by solving the time independent Schrödinger equation:

$$-\frac{\hbar^2}{2m^*}\frac{d^2y(x)}{dx^2}+V(x)y(x)=Ey(x) \qquad (1)$$

Where the $y(x)$ is the wave function as a function of the position x,

$V(x)$ is the potential distribution of the potential barrier,

E is the electron energy,

m^* is the effective mass of electron,

$\hbar$ is the reduced Planck constant.

However, this equation can be solved only for some simple potential distributions as shown in Fig. 2.1:

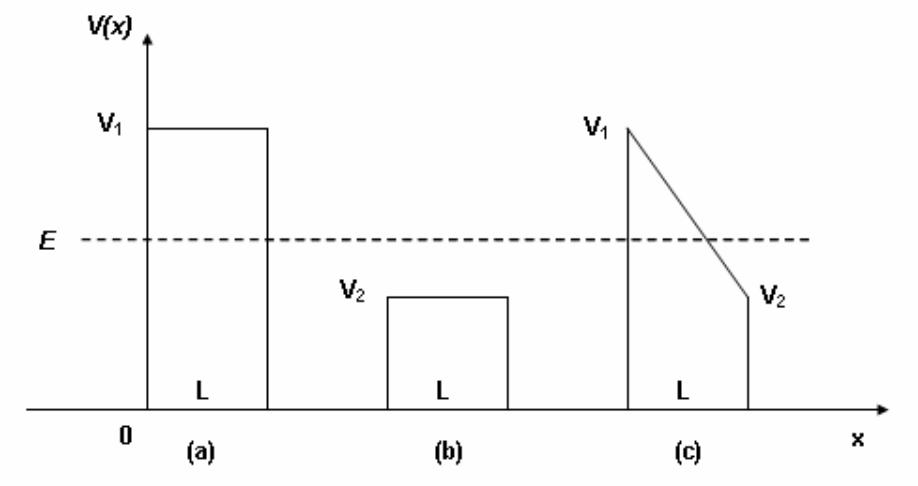

Fig. 2.1 Electron Transmission through Various Potentials

For the square barrier illustrated in Fig. 2.1(a), the potential distribution is simply

given as $V(x) = V_1$, and (1) is reduced to

$$\frac{d^2y}{dx^2} = \frac{2m^*(V_1 - E)}{\hbar^2}y \tag{2}$$

The solution of this equation is

$$y(x) = C^+e^{k_1x} + C^-e^{-k_1x} \tag{3}$$

Where k_1 is the wave number given as

$$k_1 = \sqrt{\frac{2m^*(V_1 - E)}{\hbar^2}} \tag{4}$$

For the barrier illustrated in Fig. 2.1(b) having the potential smaller than the electron energy $V_2 < E$, the Schrödinger equation should be written as

$$\frac{d^2y}{dx^2} = -\frac{2m^*(E - V_2)}{\hbar^2}y \tag{5}$$

and the corresponding solution and wave number become

$$y(x) = C^+e^{ik_2x} + C^-e^{-ik_2x} \tag{6}$$

$$k_2 = \sqrt{\frac{2m^*(E - V_2)}{\hbar^2}} \tag{7}$$

For the trapezoidal barrier illustrated in Fig. 2.1(c), the potential distribution in the barrier can be expressed as

$$V(x) = V_1 - \frac{V_1 - V_2}{L}x \tag{8}$$

Where L is the width of the trapezoidal barrier. Under this condition, the Schrödinger equation (1) can be expressed as:

$$\frac{d^2y}{dx^2} = \frac{2m^*}{\hbar^2}\frac{V_1 - V_2}{L}(h - x)y = 0 \tag{9}$$

Where

$$h = \frac{L}{V_1 - V_2}(V_1 - E) \tag{10}$$

Let

$$r(x) = \left(\frac{2m^*}{\hbar^2} \frac{V_1 - V_2}{L} \right)^{1/3} [-x + h] \tag{11}$$

then (9) transforms to

$$\frac{d^2 y}{dr^2} = r\, y\,(r) \tag{12}$$

The typical solution to this differential equation is the Airy Function [9,11]:

$$y\,(r) = C^+ Ai\,(r) + C^- Bi\,(r) \tag{13}$$

Where $Ai(x)$ is the Airy function of the first kind and $Bi(x)$ is the Airy function of second kind or complementary Airy function. The detail are described in section 3.2

2.2 Transfer Matrix for a Single Barrier

Let us consider a trapezoidal potential barrier shown in Fig. 2.2.

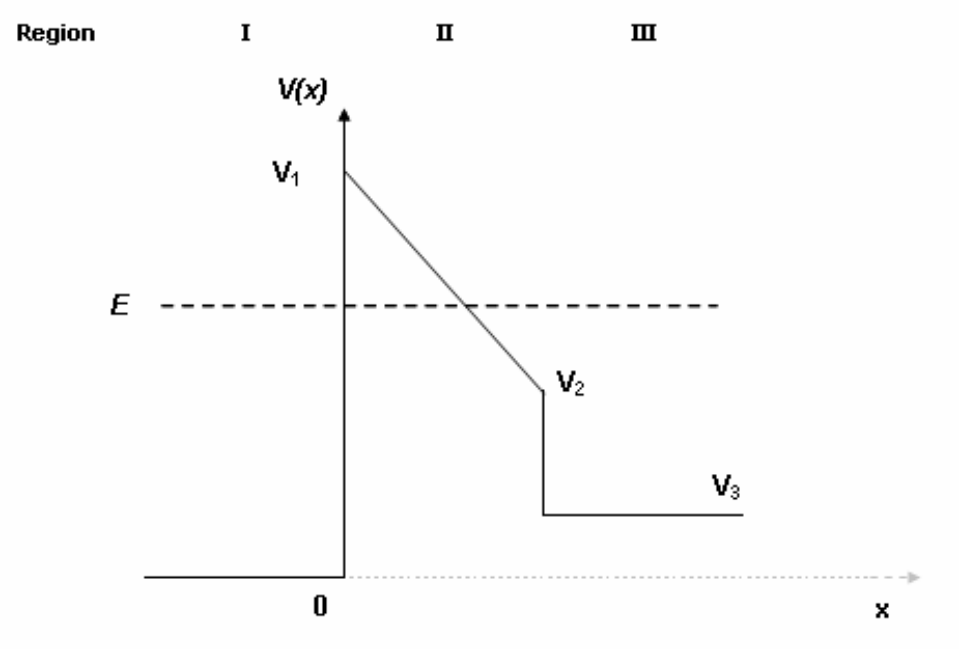

Fig. 2.2 Trapezoidal Potential Barrier

There are three regions in this barrier. In region I, the solution of wave equation is given by (6) and can be written as

$$y_1(x) = e^{ik_1 x} + \mathrm{Re}^{-ik_1 x} \tag{14}$$

$$k_1 = \sqrt{\frac{2m_1 E}{\hbar^2}} \tag{15}$$

In region II, the wave solution is given by (13)

$$y_2(r(x)) = C_2^+ Ai(r(x)) + C_2^- Bi(r(x)) \tag{16}$$

$$r(x) = \left(\frac{2m_2}{\hbar^2}\frac{V_1 - V_2}{L}\right)^{1/3}[h - x] \tag{17}$$

$$h = \frac{L}{V_1 - V_2}(V_1 - E) \tag{18}$$

In region III, we have

$$y_3(x) = Te^{ik_3 x} \tag{19}$$

$$k_3 = \sqrt{\frac{2m_3(E - V_3)}{\hbar^2}} \tag{20}$$

The transfer matrix for a single barrier can be obtained by using the continuity of wave functions as well as its slope at both boundaries of the barrier. At the boundary between region I and region II, the continuity conditions are:

$$1 + R = C_2^+ Ai(r(0)) + C_2^- Bi(r(0)) \tag{21}$$

$$ik_1(1 - R) = C_2^+ Ai'(r(0)) + C_2^- Bi'(r(0)) \tag{22}$$

The continuity conditions at the boundary between region II and region III are:

$$C_2^+ Ai(r(L)) + C_2^- Bi(r(L)) = T \tag{23}$$

$$C_2^+ Ai'(r(L)) + C_2^- Bi'(r(L)) = ik_3 T \tag{24}$$

In matrix forms, (21) to (24) may be written as

$$\begin{bmatrix} 1 & 1 \\ ik_1 & -ik_1 \end{bmatrix} \begin{bmatrix} 1 \\ R \end{bmatrix} = \begin{bmatrix} Ai(r(0)) & Bi(r(0)) \\ Ai'(r(0)) & Bi'(r(0)) \end{bmatrix} \begin{bmatrix} C_2^+ \\ C_2^- \end{bmatrix} \tag{25}$$

$$\begin{bmatrix} Ai(r(L)) & Bi(r(L)) \\ Ai'(r(L)) & Bi'(r(L)) \end{bmatrix} \begin{bmatrix} C_2^+ \\ C_2^- \end{bmatrix} = \begin{bmatrix} 1 \\ ik_3 \end{bmatrix} T \tag{26}$$

Eliminating the C_2 vector from matrix equations (25) and (26), we get the transfer matrix equation

$$\begin{bmatrix} 1 & 1 \\ ik_1 & -ik_1 \end{bmatrix} \begin{bmatrix} 1 \\ R \end{bmatrix} = M_2 \begin{bmatrix} 1 \\ ik_3 \end{bmatrix} T \tag{27}$$

where

$$M_2 = \begin{bmatrix} Ai(r(0)) & Bi(r(0)) \\ Ai'(r(0)) & Bi'(r(0)) \end{bmatrix} \begin{bmatrix} Ai(r(L)) & Bi(r(L)) \\ Ai'(r(L)) & Bi'(r(L)) \end{bmatrix}^{-1} \tag{28}$$

Note that this matrix is defined as the transfer matrix for region II and is a characteristic matrix for a trapezoidal barrier using the Airy function solution.

The transfer matrix for the square well using the exponential function can be derived in a similar way. For the case of an electron tunneling through a square barrier as shown Fig. 2.1 (a), we get the transfer matrix of evanescent wave solution

$$M_2 = \begin{bmatrix} 1 & 1 \\ k_2 & -k_2 \end{bmatrix} \begin{bmatrix} e^{k_2 L} & e^{-k_2 L} \\ k_2 e^{k_2 L} & -k_2 e^{-k_2 L} \end{bmatrix}^{-1}$$

$$= \begin{bmatrix} \cosh(k_2 L) & -\frac{1}{k_2}\sinh(k_2 L) \\ -k_2 \sinh(k_2 L) & \cosh(k_2 L) \end{bmatrix} \quad (29)$$

While for the case of an electron transmission over a square barrier as shown Fig. 2.1 (b), we get the transfer matrix of plane wave solution:

$$M_2 = \begin{bmatrix} 1 & 1 \\ ik_2 & -ik_2 \end{bmatrix} \begin{bmatrix} e^{ik_2 L} & e^{-ik_2 L} \\ ik_2 e^{ik_2 L} & -ik_2 e^{-ik_2 L} \end{bmatrix}^{-1}$$

$$= \begin{bmatrix} \cos(k_2 L) & -\frac{1}{k_2}\sin(k_2 L) \\ k_2 \sin(k_2 L) & \cos(k_2 L) \end{bmatrix} \quad (30)$$

2.3 Transmission Coefficients

In general, the transfer matrix eq.(27) may be written as:

$$\begin{bmatrix} 1 & 1 \\ ik_1 & -ik_1 \end{bmatrix}\begin{bmatrix} 1 \\ R \end{bmatrix}=\begin{bmatrix} m_{11} & m_{12} \\ m_{21} & m_{22} \end{bmatrix}\begin{bmatrix} 1 \\ ik_3 \end{bmatrix}T \tag{31}$$

Multiplying out the matrices and identifying T and R as the two independent variables, we get

$$\begin{bmatrix} m_{11}+ik_n m_{12} & -1 \\ m_{21}+ik_n m_{22} & ik_1 \end{bmatrix}\begin{bmatrix} T \\ R \end{bmatrix}=\begin{bmatrix} 1 \\ ik_1 \end{bmatrix} \tag{32}$$

or

$$\begin{aligned}\begin{bmatrix} T \\ R \end{bmatrix}&=\begin{bmatrix} m_{11}+ik_n m_{12} & -1 \\ m_{21}+ik_n m_{22} & ik_1 \end{bmatrix}^{-1}\begin{bmatrix} 1 \\ ik_1 \end{bmatrix} \\ &=\frac{1}{\Delta}\begin{bmatrix} ik_1 & 1 \\ -m_{21}-ik_n m_{22} & m_{11}+ik_n m_{12} \end{bmatrix}\begin{bmatrix} 1 \\ ik_1 \end{bmatrix}\end{aligned} \tag{33}$$

where

$$\Delta = ik_1\left(m_{11}+ik_n m_{12}\right)+m_{21}+ik_n m_{22} \tag{34}$$

Therefore, the transmissivity T and reflectivity R can be obtained as

$$T=\frac{2ik_1}{ik_1\left(m_{11}+ik_3 m_{12}\right)+m_{21}+ik_3 m_{22}} \tag{35}$$

$$R=\frac{-m_{21}-ik_3 m_{22}+ik_1\left(m_{11}+ik_3 m_{12}\right)}{ik_1\left(m_{11}+ik_3 m_{12}\right)+m_{21}+ik_3 m_{22}} \tag{36}$$

The transmission coefficient Γ is defined as

$$\begin{aligned}\Gamma(E)&=T^2 \\ &=\frac{(2k_1)^2}{\left(m_{21}-k_1k_3m_{12}\right)^2+\left(k_1m_{11}+k_3m_{22}\right)^2}\end{aligned} \tag{37}$$

Square potential

For $V(x) > E$

$$m_{11} = \cosh(k_2 L), \qquad m_{12} = -\frac{1}{k_2}\sinh(k_2 L)$$

$$m_{21} = -k_2 \sinh(k_2 L), \quad m_{22} = \cosh(k_2 L)$$

The eq.(37) becomes as

$$\frac{1}{\Gamma} = \frac{1}{4}\left[\left(1+\frac{k_3}{k_1}\right)^2 \cosh^2(k_2 L) + \left(\frac{k_3}{k_2} - \frac{k_2}{k_1}\right)^2 \sinh^2(k_2 L)\right] \tag{38}$$

For $E > V(x)$

$$m_{11} = \cos(k_2 L), \qquad m_{12} = -\frac{1}{k_2}\sin(k_2 L)$$

$$m_{21} = k_2 \sin(k_2 L), \quad m_{22} = \cos(k_2 L)$$

The eq.(37) becomes as

$$\frac{1}{\Gamma} = \frac{1}{4}\left[\left(1+\frac{k_3}{k_1}\right)^2 \cos^2(k_2 L) + \left(\frac{k_3}{k_2} - \frac{k_2}{k_1}\right)^2 \sin^2(k_2 L)\right] \tag{39}$$

2.4 WKB approximation for Arbitrary Potential

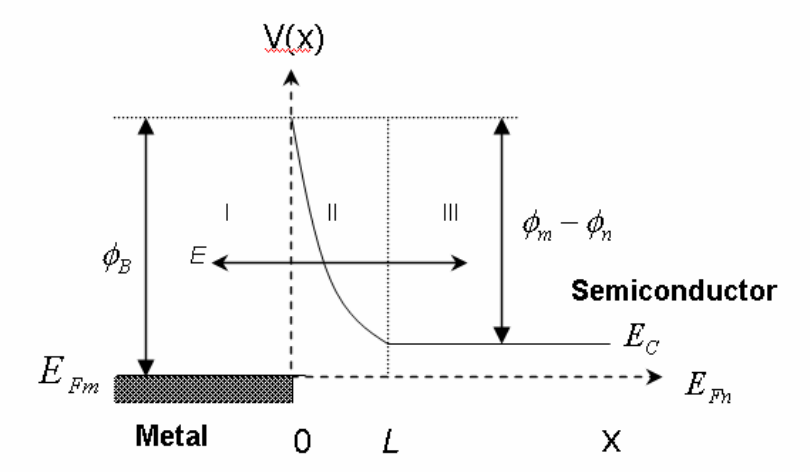

Fig. 2.4.1 Potential distribution of Schottky barrier

The WKB phase integral approximation or method is known to approximate a real Schrödinger wave function by a sinusoidal oscillation whose phase is given by the space integral of the classical momentum, the phase integral, and whose amplitude varies inversely as the fourth root of the classical momentum. This approximation was already known for the physical waves of optics and acoustics, and was quickly applied to the new Schrödinger "probability" waves.

Base on the One-dimensional time-independent Schrödinger of equation (1)

And classical momentum $p = \sqrt{2m(E - V(x))}$ (40)

(1) can be expressed as $\frac{d^2 y(x)}{dx^2} = -\frac{p^2}{\hbar^2} y(x)$ (41)

In semiclassical region, $E > V(x)$, $p(x)$ is real. Then the solution can be written in form of

$$y(x) = A(x)\exp[if(x)] \quad (42)$$

In classical forbidden region, $V(x) > E$, and $p(x)$ is imaginary

$$y(x) = A(x)\exp[\pm f(x)] = \frac{C}{\sqrt{|p(x)|}}\exp\left[\pm\frac{1}{\hbar}\int|p(x)|dx\right] \tag{43}$$

with $A(x)$ and $f(x)$ are real function. The general solution of Schrödinger can be expressed in the following

We can separate the equation into real and imaginary part. There is no general analytic solution, but if $A(x)$ varies very slowly then the $A' \& A''$ would be very small compare to f'. We can neglect the A'' to get

$$(f')^2 = \frac{p^2}{\hbar^2} \rightarrow f = \pm\frac{1}{\hbar}\int p(x)dx \tag{44}$$

The transmission coefficient Γ can be approximated under the assumption of barrier is high or wide, $V(x) >> E$, and neglecting the reflective wave. It can be written as

$$\Gamma = |T|^2 = \exp(-2g) \quad \text{where } g = \frac{1}{\hbar}\int_0^L |p(x)|dx \text{, that is,} \tag{45}$$

$$\Gamma = e^{-2\int_0^L \sqrt{(2m/\hbar^2)[V(x)-E]}dx} \tag{46}$$

There are some assumptions in the WKB approximation method when we got the general solution. The first one is amplitude $A(x)$ variation should be small enough to make A' and A'' can be ignored compare to $f(x)$. The 2nd is, it would make the WKB approximation invalid at the turning point, $E = V(x)$. That is, $p(x) \rightarrow 0$ at the turning point, which is the key, make the solution turn into invalid. The 3rd is the WKB approximation neglects the reflected wave. This would make the

deviation of the probability compare to the numerical analysis results. The transmission coefficient is assumed to be one if the electron energy equal or above the potential distribution. This is used in the program to avoid the calculation problem at the turning point.

Base on the above limitation, we can see the WKB approximation to calculate the tunneling probability in Schottky Barrier as shown in Fig2.4.1, is less accuracy than other numerical methods of Airy function and exponential function solution.

Base on the description on section 2.2 and above, the transmission coefficient of the trapezoidal potential barrier is a function of electron energy, barrier width,. The Γ calculated by Airy function of trapezoidal barrier to electron energy, and barrier width are shown on Fig.2.5.1, and Fig.2.5.2 respectively.

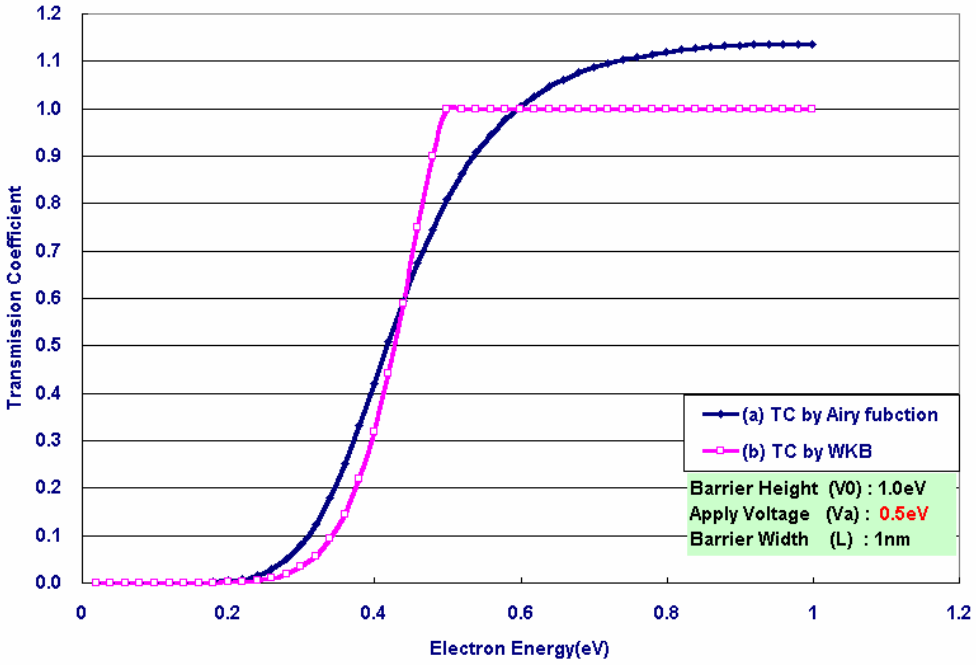

Fig.2.5.1 Transmission coefficient vs. electron energy by (a) Airy function (b) WKB approximation of trapezoidal barrier

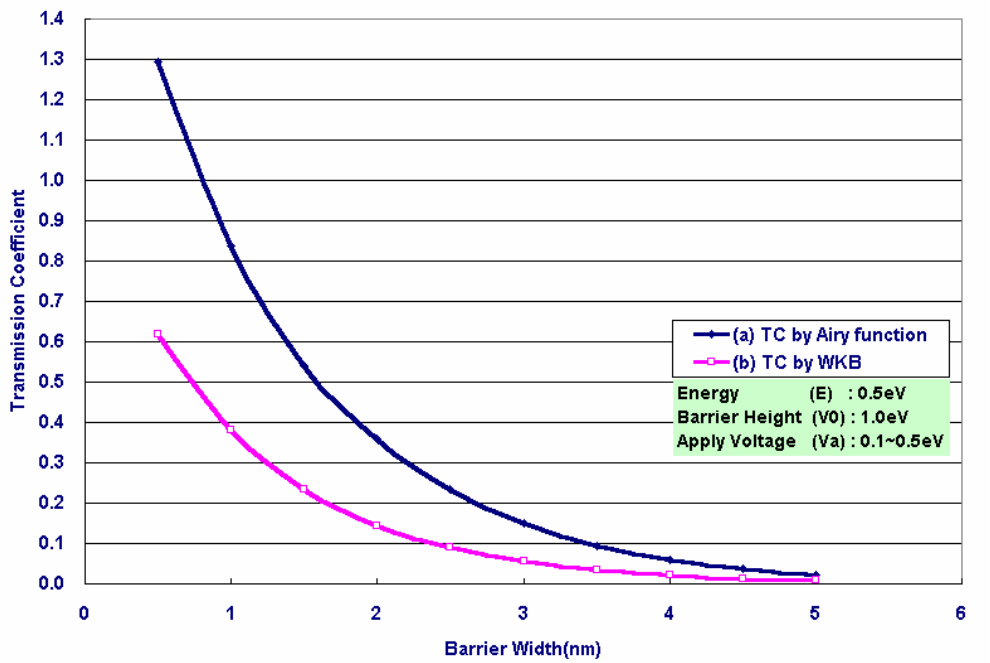

Fig.2.5.2 Transmission coefficient vs. barrier width by (a) Airy function (b) WKB approximation of trapezoidal barrier

2.5 Current through the Schottky Barrier

The current through a Schottky Barrier consists of the component flowing from metal to semiconductor J_{ms} and the component flowing from semiconductor to metal J_{sm}. For a non-degenerated semiconductor, the current density J_{ms} is proportional to the quantum mechanical transmission coefficient $\Gamma(x)$ multiplied by the occupation probability in the metal $f_m(x)$ and the unoccupied probability in semiconductor $1 - f_s(x)$:

$$J_{ms} = -qV_R N_c \int_0^{\infty} \Gamma(x) f_m(x)[1 - f_s(x)]dx \tag{47}$$

where V_R is the thermal velocity of electrons, N_c is the effective density of states in the conduction band, and $x = e/k_B T$ is the normalized electron energy. Similar expression for J_{sm} can be expressed as

$$J_{sm} = qV_R N_c \int_0^{\infty} \Gamma(x) f_s(x)[1 - f_m(x)]dx \tag{48}$$

The total current flowing across the Schottky barrier is the sum of the above two components:

$$J = -qV_R N_c \int_0^{\infty} \Gamma(x)[f_m(x) - f_s(x)]dx \tag{49}$$

However, for heavily doped degenerated semiconductor the total current flowing from metal to semiconductor is given as:

$$J = -qV_R N_c \int_0^{\infty} \Gamma(x) \ln\left[\frac{f_s(x)}{f_m(x)}\right]dx \tag{50}$$

Here $f_m(x)$ and $f_s(x)$ are the Fermi-Dirac distribution functions in the metal and

semiconductor respectively:

$$f_m(x) = \frac{1}{1+\exp(x - x_m)}, \qquad x_m = e_{Fm} \tag{51}$$

$$f_s(x) = \frac{1}{1+\exp(x - x_n)}, \qquad x_n = e_{Fn} \tag{52}$$

For a heavily doped semiconductor or for operation at low temperatures, the Schottky barrier current given in (49) and (50) actually can be divided into two components: the quantum mechanical tunneling current J_{TL} and the thermionic-emission tunneling current J_{TE}

$$J_{TL} = -qV_R N_c \int_0^{x_b} \Gamma(x) F_{ms}(x) dx \tag{53}$$

$$J_{TE} = -qV_R N_c \int_{x_b}^{\infty} \Gamma(x) F_{ms}(x) dx \tag{54}$$

where x_b is the barrier height and $F_{ms}(x)$ is the transition probability of electrons from semiconductor to meal and is given as:

$$F_{ms}(x) = f_m(x) - f_s(x) \tag{55}$$

for non-degenerate semiconductor and

$$F_{ms}(x) = \ln\left[\frac{f_s(x)}{f_m(x)}\right] \tag{56}$$

for degenerate semiconductor.

Chapter 3 . Numerical Simulation

3.1 Space Discretization

The solutions described in Chapter 2 are base on single potential barrier. If we like to demonstrate those solutions in matrix form, the potential should be divided into small areas. Each area can be treated as single potential barrier and cascade the solution as probability and transmission coefficient calculation. There are two ways to discretized the potential barrier as shown on Fig3.1.1 by piecewise linear approximation and Fig3.1.2 by step approximation. V_0 is the barrier height, V_a is the applied voltage across the barrier. b is the width of each region. L is the total width of barrier.

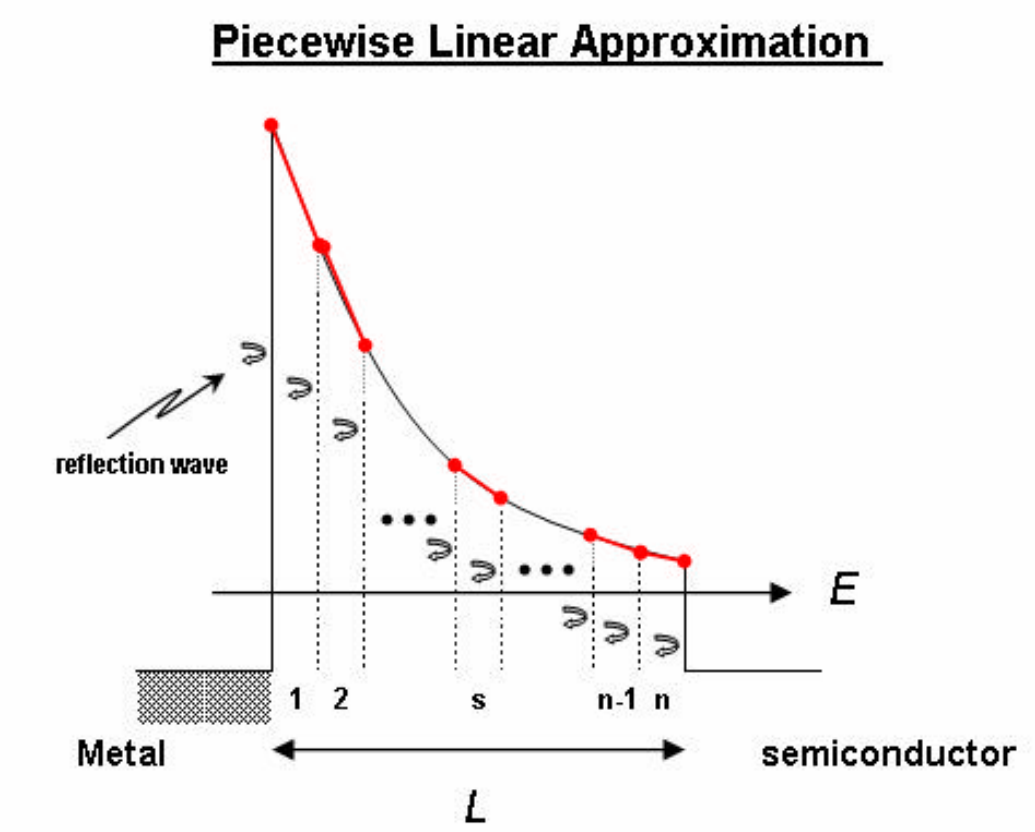

Fig3.1.1 Piecewise linear approximation for Schottky Barrier. The barrier, total depth is L, is divided into n section. S is the s^{th} section in the barrier. The Width of each barrier is b

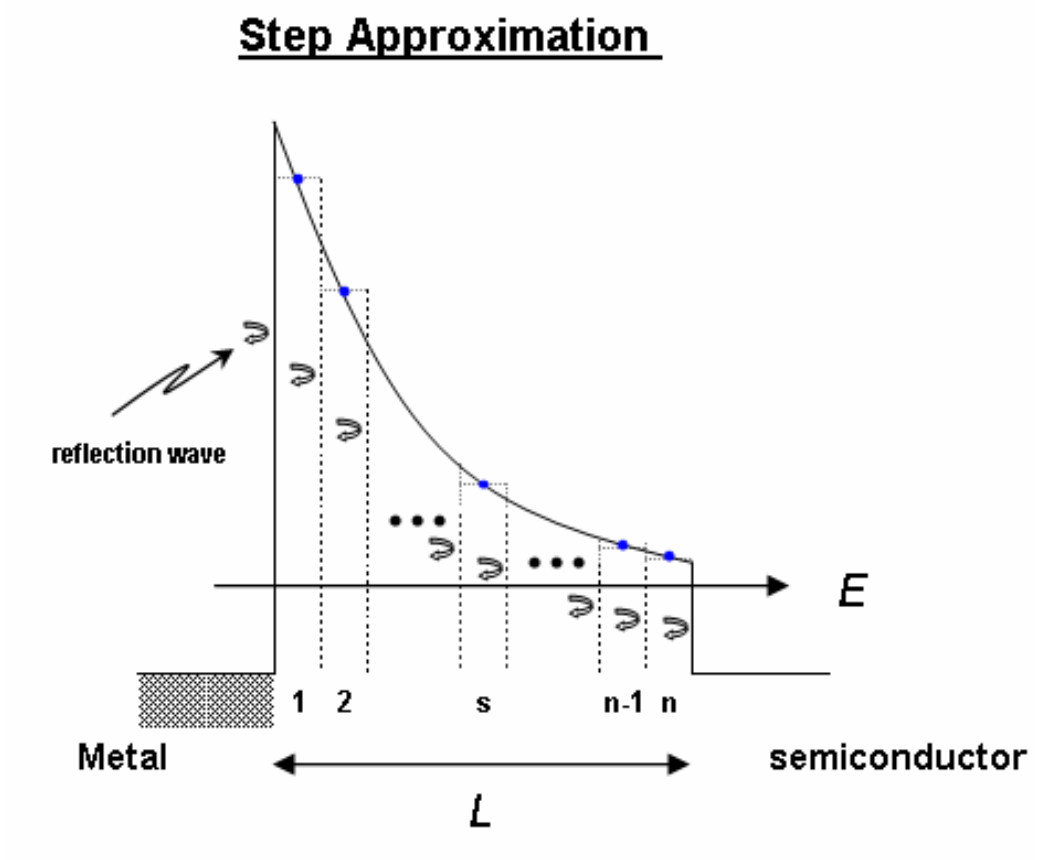

Fig3.1.2 Step approximation for Schottky Barrier. The barrier, total depth is L, is divided into n section. S is the sth section in the barrier. The width of each barrier is b

3.2 Transfer Matrix Formulation

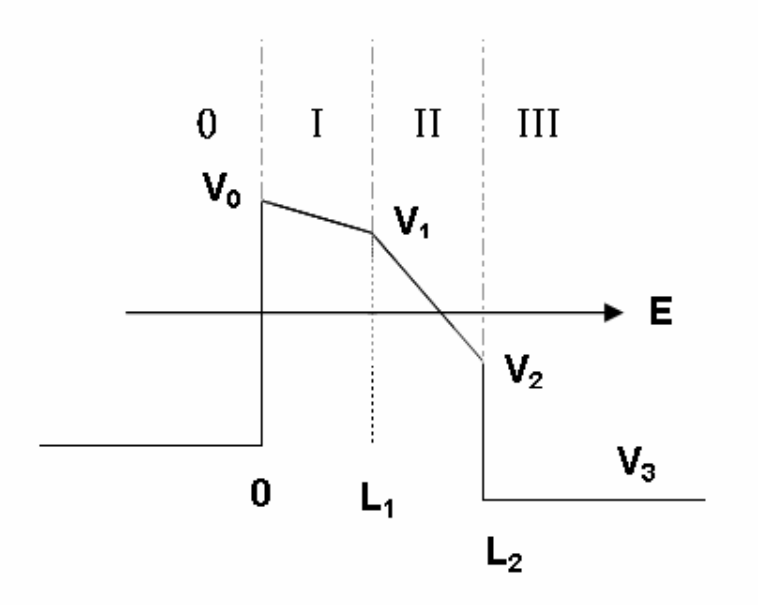

In the region 0

$$\Psi_0(x) = e^{ik_0 x} + \mathrm{Re}^{-ik_0 x} \qquad x \le 0 \tag{57}$$

$$k_0 = \sqrt{\frac{2mE}{\hbar^2}} \tag{58}$$

In the region I

$$\Psi_1(r_1) = C_1^+ Ai(r_1) + C_1^- Bi(r_1) \tag{59}$$

$$r_1(x) = \left(\frac{2m}{\hbar^2}\frac{V_0 - V_1}{L_1}\right)^{\frac{1}{3}}(-x + h_1) \quad , 0 \le x \le L_1 \tag{60}$$

$$h_1 = \frac{L_1}{V_0 - V_1}(V_0 - E) \tag{61}$$

In the region II

$$\Psi_2(r_2) = C_2^+ Ai(r_2) + C_2^- Bi(r_2) \tag{62}$$

$$r_2(x)=\left(\frac{2m}{\hbar^2}\frac{V_1-V_2}{L_2}\right)^{\frac{1}{3}}(-x+h_2) \quad , L_1 \le x \le L_2 \tag{63}$$

$$h_2=\frac{L_2}{V_1-V_2}(V_1-E) \tag{64}$$

In the region 3

$$\Psi_3(x)=Te^{ik_3x} \quad , x \ge L_2 \tag{65}$$

$$k_3=\sqrt{\frac{2m(E-V_3)}{\hbar^2}} \tag{66}$$

at boundary of regions 0 and I

$$1+R=C_1^+Ai(r_1(0))+C_1^-Bi(r_1(0)) \tag{67}$$

$$ik_0(1-R)=C_1^+Ai'(r_1(0))+C_1^-Bi'(r_1(0)) \tag{68}$$

$$\begin{bmatrix}1 & 1\\ ik_0 & -ik_0\end{bmatrix}\begin{bmatrix}1\\ R\end{bmatrix}=\begin{bmatrix}Ai(r_1(0)) & Bi(r_1(0))\\ Ai'(r_1(0)) & Bi'(r_1(0))\end{bmatrix}\begin{bmatrix}C_1^+\\ C_1^-\end{bmatrix} \tag{69}$$

at boundary of regions I and II

$$C_1^+Ai(r_1(L_1))+C_1^-Bi(r_1(L_1))=C_2^+Ai(r_2(0))+C_2^-Bi(r_2(0)) \tag{70}$$

$$C_1^+Ai'(r_1(L_1))+C_1^-Bi'(r_1(L_1))=C_2^+Ai'(r_2(0))+C_2^-Bi'(r_2(0)) \tag{71}$$

$$\begin{bmatrix}Ai(r_1(L_1)) & Bi(r_1(L_1))\\ Ai'(r_1(L_1)) & Bi'(r_1(L_1))\end{bmatrix}\begin{bmatrix}C_1^+\\ C_1^-\end{bmatrix}=\begin{bmatrix}Ai(r_2(0)) & Bi(r_2(0))\\ Ai'(r_2(0)) & Bi'(r_2(0))\end{bmatrix}\begin{bmatrix}C_2^+\\ C_2^-\end{bmatrix} \tag{72}$$

at boundary of regions II and III

$$C_2^+Ai(r_2(L_2))+C_2^-Bi(r_2(L_2))=T \tag{73}$$

$$C_2^+Ai'(r_2(L_2))+C_2^-Bi'(r_2(L_2))=ik_3T \tag{74}$$

$$\begin{bmatrix}Ai(r_2(L_2)) & Bi(r_2(L_2))\\ Ai'(r_2(L_2)) & Bi'(r_2(L_2))\end{bmatrix}\begin{bmatrix}C_2^+\\ C_2^-\end{bmatrix}=\begin{bmatrix}1\\ ik_3\end{bmatrix}T \tag{75}$$

Eliminating C_1 and C_2 from (69) to (72), we get

$$\begin{bmatrix} 1 & 1 \\ ik_0 & -ik_0 \end{bmatrix}\begin{bmatrix} 1 \\ R \end{bmatrix} = \begin{bmatrix} Ai(r_1(0)) & Bi(r_1(0)) \\ Ai'(r_1(0)) & Bi'(r_1(0)) \end{bmatrix}\begin{bmatrix} Ai(r_1(L_1)) & Bi(r_1(L_1)) \\ Ai'(r_1(L_1)) & Bi'(r_1(L_1)) \end{bmatrix}^{-1} \bullet \begin{bmatrix} Ai(r_2(0)) & Bi(r_2(0)) \\ Ai'(r_2(0)) & Bi'(r_2(0)) \end{bmatrix}\begin{bmatrix} Ai(r_2(L_2)) & Bi(r_2(L_2)) \\ Ai'(r_2(L_2)) & Bi'(r_2(L_2)) \end{bmatrix}^{-1}\begin{bmatrix} 1 \\ ik_3 \end{bmatrix} T \quad (76)$$

where M_1 and M_2 are the transfer matrix for regions I and II

$$M_1 = \begin{bmatrix} Ai(r_1(0)) & Bi(r_1(0)) \\ Ai'(r_1(0)) & Bi'(r_1(0)) \end{bmatrix}\begin{bmatrix} Ai(r_1(L_1)) & Bi(r_1(L_1)) \\ Ai'(r_1(L_1)) & Bi'(r_1(L_1)) \end{bmatrix}^{-1} \quad (77)$$

$$M_2 = \begin{bmatrix} Ai(r_2(0)) & Bi(r_2(0)) \\ Ai'(r_2(0)) & Bi'(r_2(0)) \end{bmatrix}\begin{bmatrix} Ai(r_2(L_2)) & Bi(r_2(L_2)) \\ Ai'(r_2(L_2)) & Bi'(r_2(L_2)) \end{bmatrix}^{-1} \quad (78)$$

(76) can be expressed as

$$\begin{bmatrix} 1 & 1 \\ ik_0 & -ik_0 \end{bmatrix}\begin{bmatrix} 1 \\ R \end{bmatrix} = M_1 M_2 \begin{bmatrix} 1 \\ ik_3 \end{bmatrix} T = M \begin{bmatrix} 1 \\ ik_3 \end{bmatrix} T \quad (79)$$

where $M = M_1 \cdot M_2$

Extend to n regions as shown in chapter 3.1, the matrix of s^{th} region, M_s, is represented

$$M_s = \begin{bmatrix} Ai(r_s(0)) & Bi(r_s(0)) \\ Ai'(r_s(0)) & Bi'(r_s(0)) \end{bmatrix}\begin{bmatrix} Ai(r_s(L_s)) & Bi(r_s(L_s)) \\ Ai'(r_s(L_s)) & Bi'(r_s(L_s)) \end{bmatrix}^{-1} \quad (80)$$

Extending to n+1 regions, we have

$$\begin{bmatrix} 1 & 1 \\ ik_0 & -ik_0 \end{bmatrix}\begin{bmatrix} 1 \\ R \end{bmatrix} = M_1 M_2 M_3 \cdots M_n \begin{bmatrix} 1 \\ ik_n \end{bmatrix} T = M \begin{bmatrix} 1 \\ ik_n \end{bmatrix} T \quad (81)$$

where

$$M = M_2 M_3 \cdots M_{n-1} = \prod_{s=2}^{n-1} M_s \tag{82}$$

3.3 Discretization of Device Equations

Device Equations

The electrical properties of semiconductor device can be completely specified by physical relationship. They are 1) Poisson' equation, 2) electron and hole transport equations, 3) Electron and hole continuity equations. Applying the boundary conditions can solve current density, electron potential, and carrier concentration.

Poisson Equation

$$\frac{d^2y}{dx^2} = \frac{-q}{e_{Si}}\left(p - n + N\right) \tag{83}$$

Transport Equations

$$J_n = qm_n nE_x + qD_n \frac{dn}{dx} \tag{84}$$

$$J_P = qm_p pE_X - qD_p \frac{dp}{dx} \tag{85}$$

Continuity Equations

$$\frac{dn}{dt} = \frac{1}{q}\frac{dJ_n}{dx} - U \tag{86}$$

$$\frac{dp}{dt} = -\frac{1}{q}\frac{dJ_p}{dx} - U \tag{87}$$

where n and p, J_n ad J_p, m_n and m_P are the concentrations, current densities, and mobility of electrons and holes, respectively. *U* is the recombination rate, q is the electron charge, *E* is the electric field, y is the space charge potential. e_{Si} is the permittivity of semiconductor.

The main consideration in selecting a solution algorithm is the convergence properties of discretized equation and the iterative sequence. The Poisson equation is discretized and solved simultaneous with continuity equation and substituted into Transport equation to calculate the current density. The discretized procedure of Poission equation of n type semiconductor can be illuminated as

$$\frac{y_{i+1}}{\Delta X_2} - y_i\left(\frac{1}{\Delta X_2}+\frac{1}{\Delta X_1}\right)+\frac{y_{i-1}}{\Delta X_1} = -p_i + n_i - N_i \tag{88}$$

where

$\Delta X_1 = \Delta X_i(\Delta X_{i+1} + \Delta X_i)/2$ and $\Delta X_2 = \Delta X_{+1i}(\Delta X_{i+1} + \Delta X_i)/2$

To discretized the continuity equation between the initial time t_0 and final time t_1, the equations can be written as

$$\frac{n_i(t_1) - n_i(t_0)}{\Delta t} = \frac{J_n\left(i+1/2\right) + J_n\left(i-1/2\right)}{[\Delta x(i+1) + \Delta x(i)]/2} + G_i \tag{89}$$

$$\frac{p_i(t_1) - p_i(t_0)}{\Delta t} = \frac{J_p\left(i+1/2\right) + J_p\left(i-1/2\right)}{[\Delta x(i+1) + \Delta x(i)]/2} + G_i \tag{90}$$

The J_n of between i to i+1 section can be presented by discretized the Current Transport equation as

$$J_n\left(i+1/2\right) = m_n\left(i+1/2\right)E\left(i+1/2\right)\left[\frac{n(i+1)}{1-\exp\left(-E\left(i+1/2\right)\Delta x(i+1)\right)} + \frac{n(i)}{1-\exp\left(E\left(i+1/2\right)\Delta x(i+1)\right)}\right] \tag{91}$$

3.4 Boundary Conditions

The boundary conditions of the device equations at the metal semiconductor interface are used for the thremionic emission current calculation. The barrier height, f_B, including a voltage drop, Δf across the interfacial layer is the Schottky effect induced barrier lowering.

Barrier lowering

The Schottky effect, which is the image force induced lowering of the potential energy carrier emission when an electric field x is applied. The energy-band diagram between a metal surface and Semiconductor is shown on Fig3.4. A voltage drop, Δf is the barrier lowering and the thickness of the interfacial layer, Xm. To make the image force deviation by x equal to zero can get the Δf by Schottky barrier lowering, effect can be expressed as

$$\Delta f = \sqrt{\frac{qx}{4pe_s}} = 2xXm \quad \text{V} \tag{92}$$

$$Xm = \sqrt{\frac{q}{16pe_s x}} \quad \text{cm} \tag{93}$$

Where x is applied electrical field

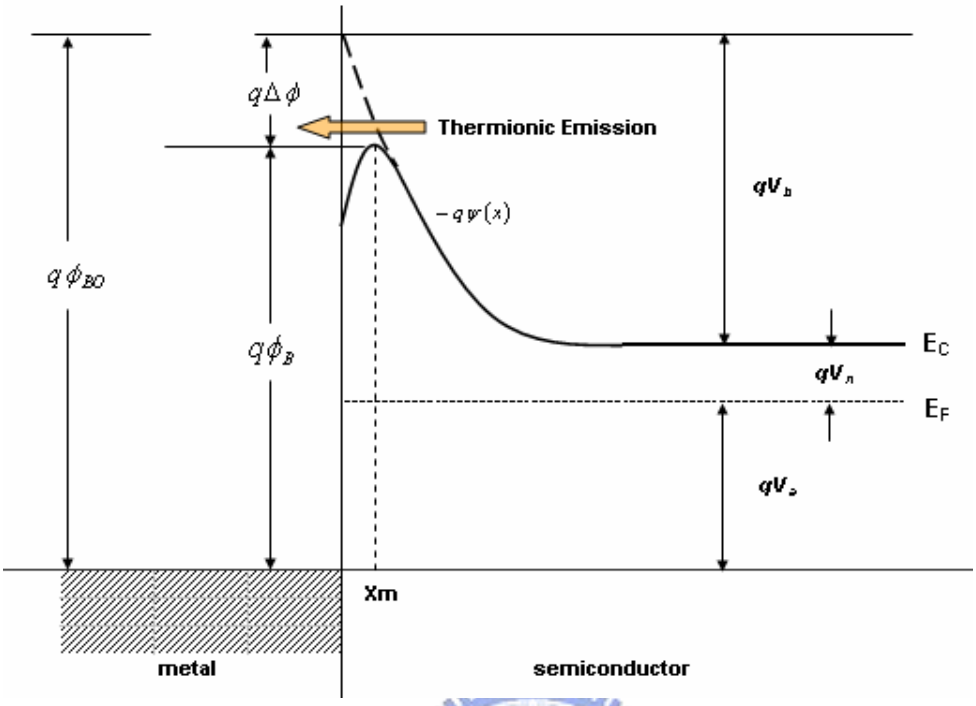

Fig 3.4 Energy Band diagram of metal-n type semiconductor junction under forward-biased condition, where $y(x)$ is the Schottky potential profile, f_B is the total effective barrier height for thermoinic emission, Δf is the total barrier lowering.

The thermionic emission current, J_{TE}, which is calculated at the grid of the interface between the metal and semiconductor for the electron energy over the barrier height.

$$J_{TE} = -qV_R N_c \int_{x_b}^{\infty} \Gamma(x) F_{ms}(x) dx \qquad (94)$$

where $x_b = qf_b$

3.5 Generation Rate

The thermoinic -emission process occurs at the interface of metal-semiconductor and the tunneling happen in bulk region which is away from the interface. A self-consistent calculation is introduced to well link the tunneling process and thermoinic -emission process with all current transport through the Schottky barrier. The key to calculate the tunneling current through the barrier is converted into a local generation or recombination process where the local generation rate, $G(x)$, depend on the local Fermi-level and potential profile, $y(x)$, along the tunneling path. The tunneling integral over distance and energy can be transformed into double integral over distance along as Fig.3.5.[1]

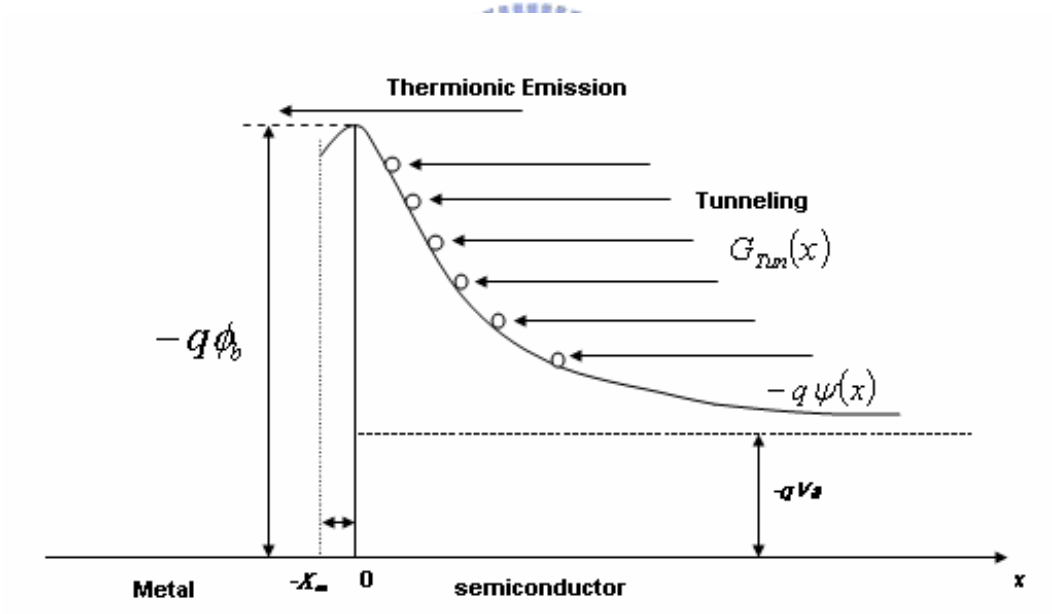

Fig 3.5. Generation rate due to tunneling in the bulk of the barrier and thermoinic emission at the metal-semiconductor interface.

For n type semiconductor, the local generation rate, G, can be expressed as

$$G(x) = \frac{1}{q}\frac{dJ_{TL}}{dx} = \frac{1}{q}\frac{dJ_{TL}}{dy}\frac{dy}{dx} = \frac{dJ_{TL}}{de}\cdot\vec{E} \qquad (95)$$

where y , $e = -qy$, $\vec{E} = -\frac{dy}{dx}$ are the electrostatic potential, energy level and the electric field respectively. Use (71) and note that $x = e / k_B T$, $e = -qy$ and $E = -dy / dx$, we have

$$dx = -\frac{q}{k_B T} dy = \frac{qE}{k_B T} dx \tag{96}$$

where *E* is the local electric field. Using (96) in (53) the energy integral becomes the space integral:

$$J_{TL} = \frac{q^2 V_R N_c}{k_B T} \int_0^L \Gamma(x) F_{ms}(x) E dx \tag{97}$$

Substitute into (95) the local generation rate can be expressed as

$$G(x) = \frac{1}{q} \frac{dJ_{TL}}{dx} = \frac{qV_R N_c}{k_B T} \Gamma(x) F_{ms}(x) E \tag{98}$$

Chapter 4 Results & Discussion

4.1Transmission Coefficient

Different numerical models have been presented to calculate the transmission coefficient, TC, in chapter 2. The WKB approximation is widely used to solve the Schrödinger equation under some assumptions, which make it is not expected to be so accurate. Besides, the WKB method is invalid at the turning point, which is the electron energy equal to the Schottky barrier potential distribution, $E(x)=V(x)$. However, the Airy function and exponential function models for descritized Scottky barrier shown in Fig.3.1.1 and Fig.3.1.2 provide more accurate simulation results than WKB approximation model. The transmission coefficient calculation by transfer matrix form of Airy Function solutions are described on (79) to (82)

The simulation results as in Fig.4.1.1 show the difference around those three models. In WKB approximation, TC is assumed to be one when the electron energy above the barrier height at the interface and decrease as a function of electron energy. The Airy function and exponential function models provide the TC simulation result even the electron energy above the barrier height. This unique finding allows a unified simulation of harmonic emission current discussed in section 4.4.

The concept for Airy function model is shown on the Fig.3.1.1 of linear piecewise and exponential method simulation on Fig.3.1.2 of step approximation. Theoretically, it is more accurate by using linear piecewise approach. However, if the **n** sections in Fig.3.1.1 and Fig.3.1.2 are large enough, the difference between Airy function and exponential methods would be almost non-visible as the results shown in Fig.4.1.1.

The potential of the Schottky barrier, $V(x)$ decrease along the barrier depth which make the absolute value of classical momentum of (3) decrease as well which result in smaller TC as shown in Fig.4.1.3. Moreover, the WKB approximation simulation result is smaller than the simulated result by Airy function under degenerated semiconductor

of 10^{20} cm^{-3} doping concentration.

The transmission is an increasing function of doping concentration. The potential distribution is more shaper due to the quansi-Fermi-level of n type semiconductor, E_f closing to conduction band, E_C as shown in Fig 4.1.2.

Base on the above discussion, The Airy function and exponential function models provides more accurate result than WKB approximation model and capably to calculated the TC for the electron energy above the barrier height where a unified simulation is proposed.

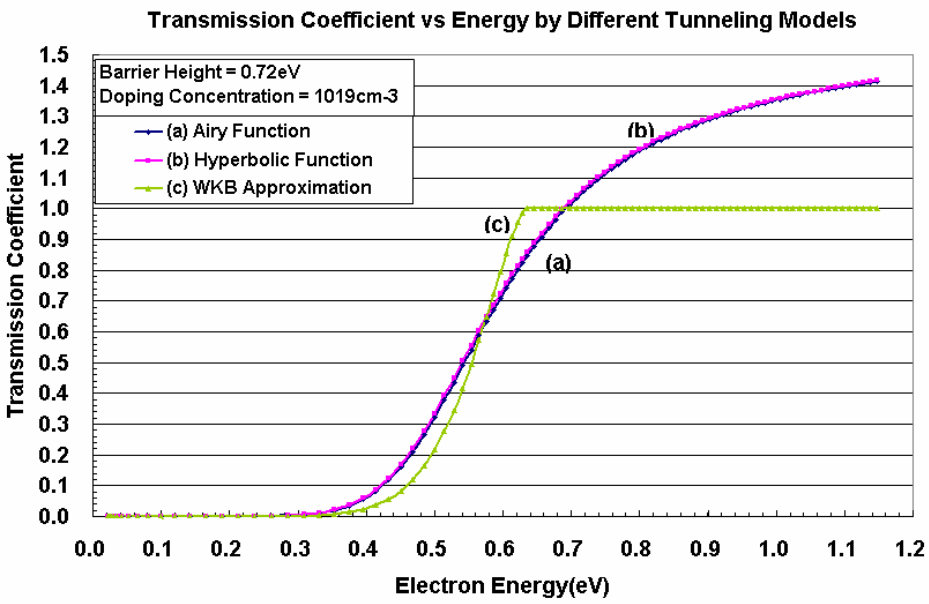

Fig 4.1.1 Transmission coefficient vs electron energy calculated by **(a)** Airy function solution **(b)** exponential solution **(c)** WKB approximation under conditions of barrier height 0.72eV and doping concentration $10^{19}cm^{-3}$ at zero apply voltage

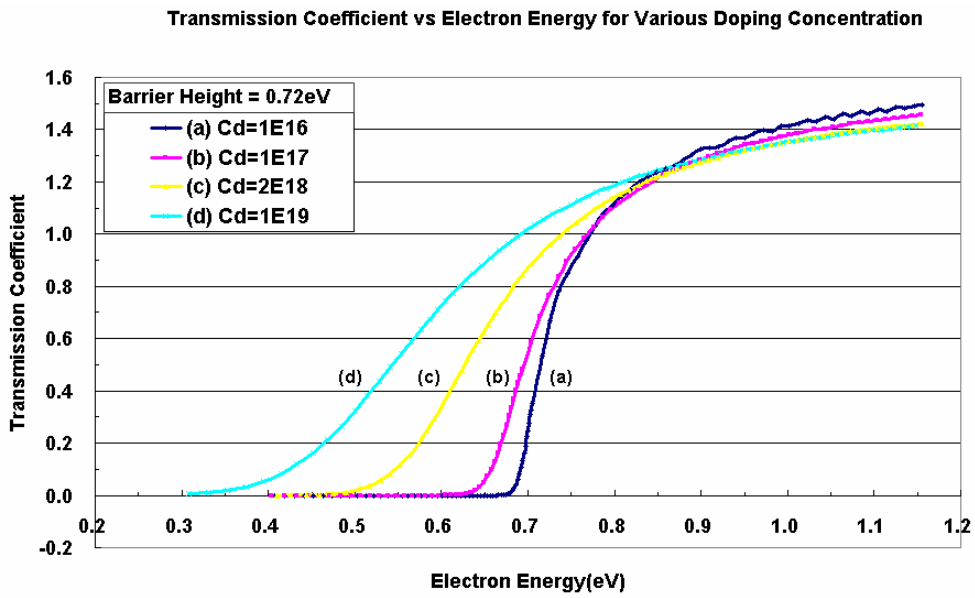

Fig 4.1.2 Transmission coefficient vs electron energy calculated by Airy function solution for doping concentration of **a)** 10^{16} cm^{-3}, **b)** 10^{17} cm^{-3}, **c)** $2*10^{18}$ cm^{-3}, **d)** 10^{19} cm^{-3} under conditions of barrier height=0.72eV at zero apply voltage

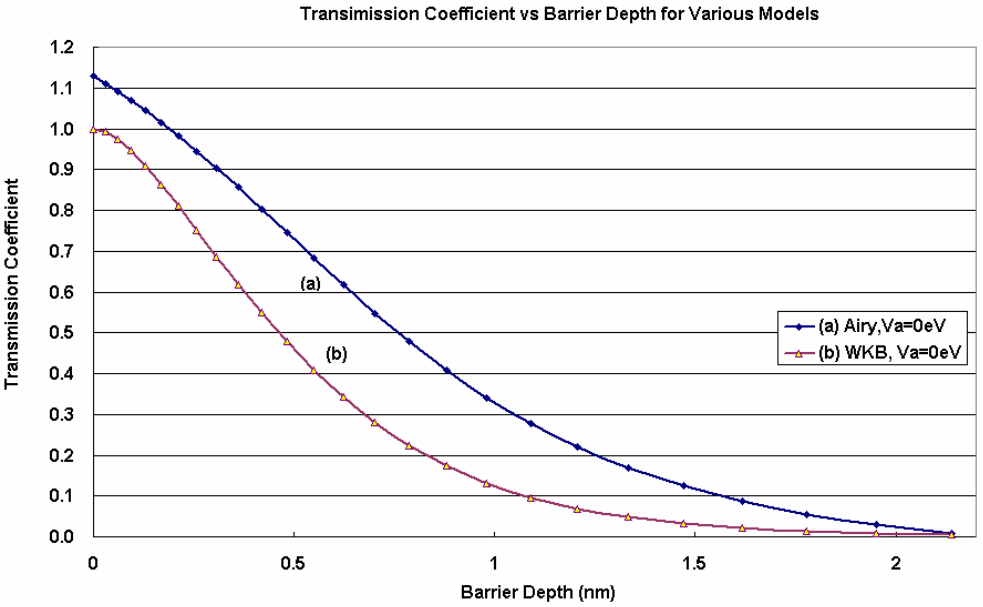

Fig 4.1.3 Space distribution of transmission coefficient calculated by **(a)** Airy function and **(b)** WKB approximation, under conditions of barrier height 0.72eV , doping concentration= $10^{20}cm^{-3}$ and zero apply voltage

4.2 Transition Probability

The local generation rate,GR, which is the function of transmission coefficient, transition probability and electric field as shown in (98). Most of the discussion base on the p+ or n+ semiconductor, which is called non-degenerated model, but not for higher doping concentration of $N > N_C$, which is degenerated semiconductor. The different degeneracy models of Maxwell-Boltzmann distribution, degeneracy and non-degeneracy models are discussed. The Maxwell-Boltzmann distribution in the metal and semiconductor are described in (47) and (48). The transition probabilities by non-degenerated and degenerated models are described in (55) and (56).

For higher doping concentration of n type semiconductor, the occupied probability $f_s(x)$ is getting smaller and result in larger transition probability F_{ms}. The transition probabilities of different degeneracy models are shown in Fig.4.2.1. and Fig4.2.2. The transition probabilities are almost identical at lower doping concentration no matter by which degeneracy models. The difference can be seen away interfacial layer at higher doping concentration condition. The non-degenerate model may not be accurate for the degenerate semiconductor of doping concentration over $N > N_C$ where the Fermi-level is over the conduction band on degenerated semiconductor. Even though the transition probability by degenerated model is higher than non-degenerated model, the contribution to total current density is relative small due to the combination effect of electric field, transition probability and transmission coefficient which discussed in section 4.3. Base on the comparison, the degeneracy models is suitable for the simulation of Schottky to Ohmic contacts as the impurity concentration is increased.

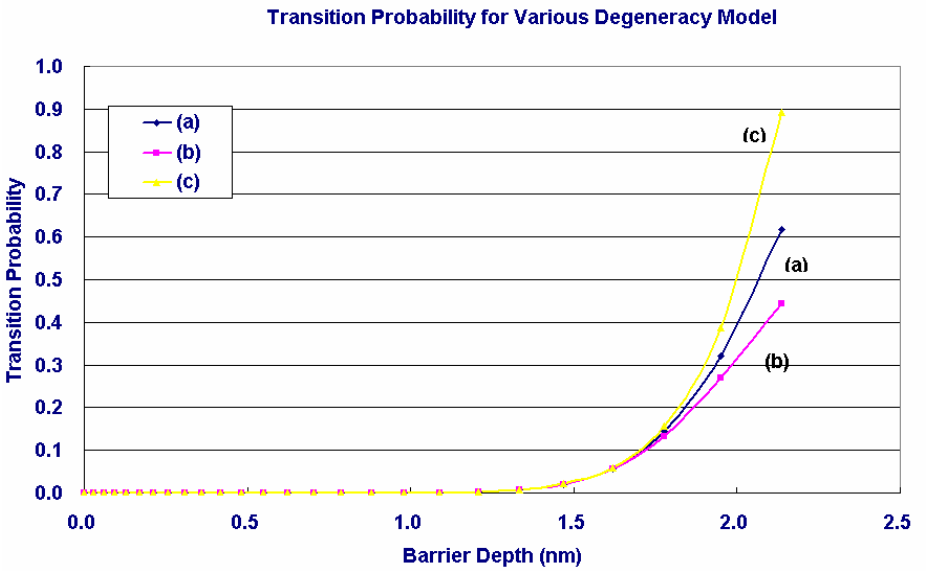

Fig 4.2.1 Space distribution of transition probability by using **a)** Degenerated model **b)** Non-degenerated model ,and **c)** Maxwell-Bolzman model under conditions of doping concentration 10^{19} cm^{-3}, apply voltage 0.2eV and barrier height 0.72eV

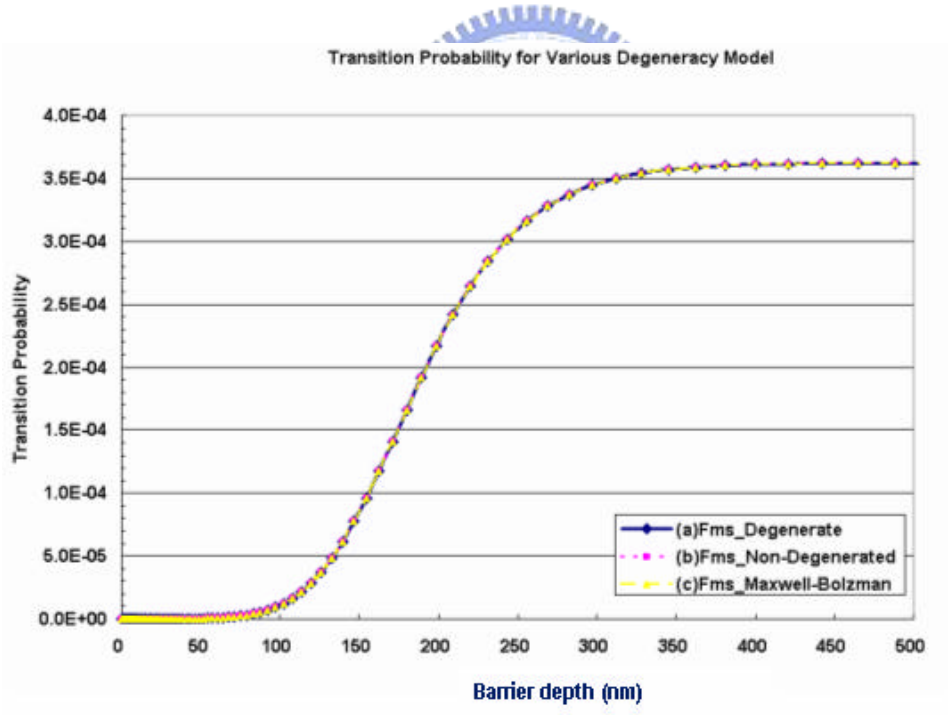

Fig 4.2.2 Space distribution of transition probability under conditions of doping concentration 10^{16} cm^{-3}, apply voltage=0.2eV and barrier height=0.72eV using **a)** Degenerated model **b)** Non-degenerated model **c)** Maxwell-Bolzmann model

4.3 Generation Rate

The local generation rate as show in (98) represents the tunneling current along the barrier depth. The total tunneling current is to integrate the tunneling current along the X space from interfacial layer till the electron energy larger than barrier potential. The generation rate is consistence increasing or decreasing along the X space since it is the function of three components, electric field, transition probability and transmission coefficient. The maximum generation rate happen at the cross point of transition probability and transmission coefficient as shown on Fig 4.3.1 of doping concentration 10^{19} cm^{-3}. Base on the discussion on section 4.1 and 4.2, the doping concentration is the factor to influence $\Gamma(x)$ and $F_{ms}(x)$. The potential distribution, $V(x)$ and quasi Fermi-level, x_n. The $\Gamma(x)$ degraded rapidly along X space and mainly contribute to generation rate as shown on Fig.4.3.2 of doping concentration 10^{16} cm^{-3}. It is realized that the tunneling current most happen between the interfacial layer and few nm of barrier depth. In this device condition we discussed, it is about 10nm. The other point is that the maximum tunneling current is few nm away interfacial layers on higher doping concentration due to the combination effect of transmission coefficient, transition probability and electric field.

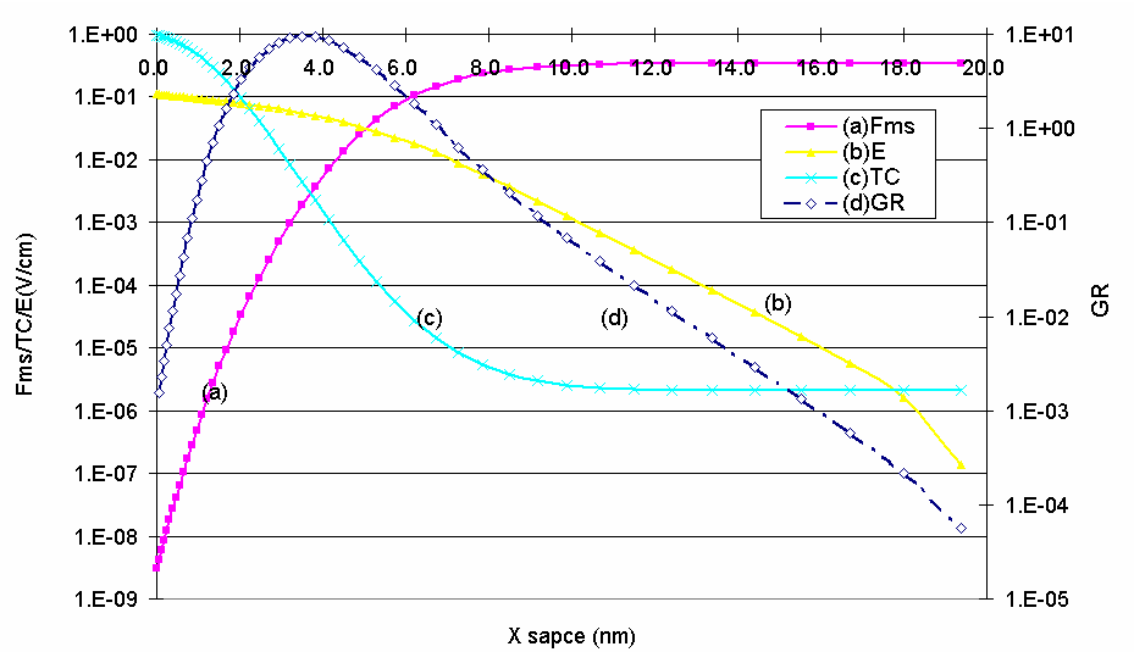

Fig 4.3.1 Spatially distribution of **(a)** transition probability **(b)** electric field, **(c)** transmission coefficient, and **(d)** generation rate under conditions of barrier height 0.72eV and Cd 10^{19} cm^{-3} and apply voltage 0.2eV, (Log scale for both Y1 & Y2 axies)

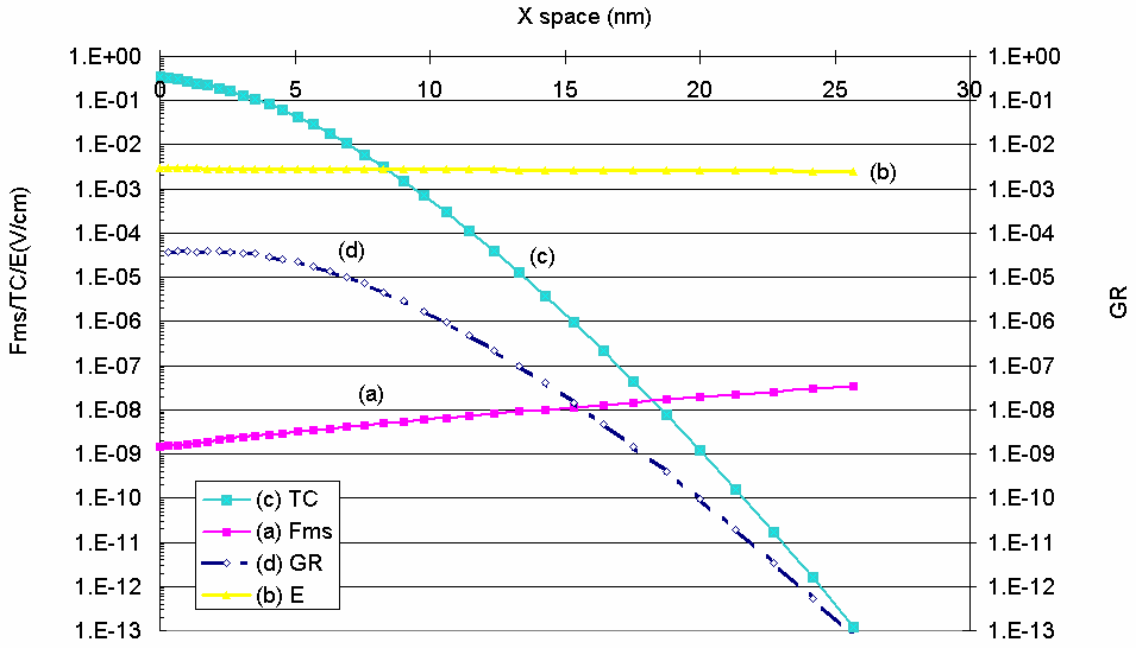

Fig 4.3.2 Spatially distribution of **(a)** transition probability **(b)** electric field, **(c)** transmission coefficient, and **(d)** generation rate under conditions of barrier height 0.72eV and Cd 10^{16} cm^{-3} and apply voltage 0.2eV, (Log scale for both Y1 & Y2 axies)

4.4 Current Density

4.4.1 Tunneling Current, J_{TL}

The current density through the Schottky barrier include the thermionic emission at the metal/semiconductor interface and the spatially distribution tunneling calculated at each grid of semiconductor around the interface. The generation rate is used to calculate the tunneling current as shown on (54),(98). The energy band diagram of Schottky Barrier in thermal equilibrium condition is showed in Fig.2.4.1. The fermi-level of metal and semiconductor are equal to each other, that is, $x_m = x_n$. The transition probability of (55) and (56) turn to zero and result in zero current density. The barrier height decrease as a forward bias,V_a, is applied, Since the generation rate is the increasing function of electric field, which is increased by apply voltage. The current density is an increasing function of apply voltage as shown on Fig 4.4.1. The difference between forward and reverse bias is due to the relative barrier height increased by reverse bias, which decrease the transmission coefficient and result in lower current density than forward bias. The thermionic emission can represent the total current at lower impurity concentration or under lower bias conditions but insufficient when the tunneling phenomena is dominant. This phenomena is illuminated in Fig4.2.2 of the ratio of tunneling current to total current density. The tunneling current is the dominated at the impurity concentration of 10^{19} cm^{-3} compare to lower impurity doping concentration of 10^{16} cm^{-3}. In brief, the current density increased by applies voltage. The tunneling effect is the dominant contribution to total current density at higher impurity concentration.

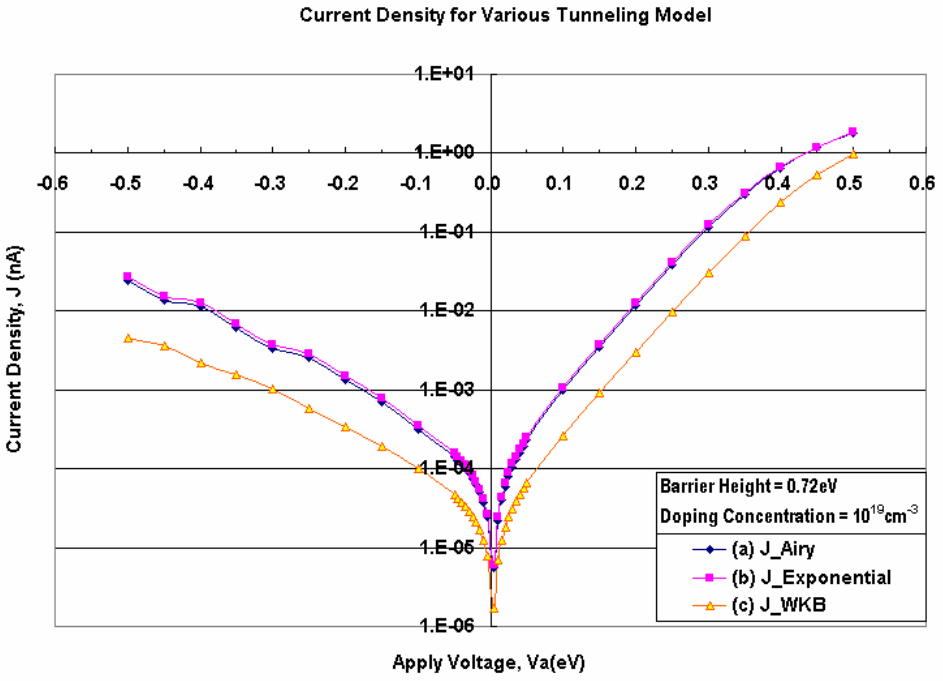

Fig 4.4.1 Current density vs apply voltage calculated by **(a)** Airy function solution **(b)** exponential function s olution **(c)** WKB approximation under conditions of barrier height 0.72eV and doping concentration 10^{19} cm^{-3}

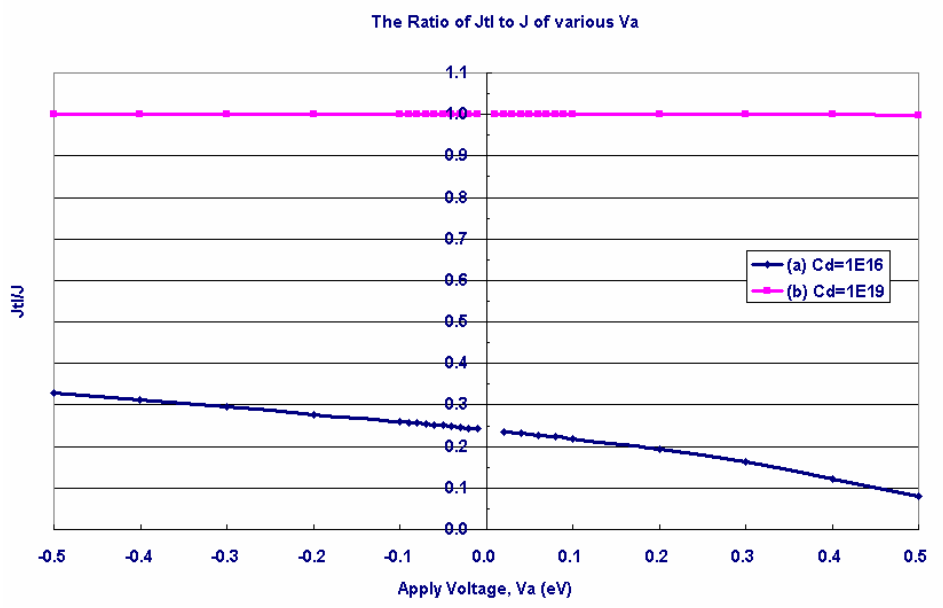

Fig. 4.4.2 The ratio of tunneling current, J_{TL} to total current, J, vs apply voltage under condition of **a)** Cd=10^{16} cm^{-3} **b)** Cd= 10^{19} cm^{-3} and barrier height 0.72eV

4.4.2 Thermionic Emission Current, J_{TE}

The thermionic emission current is calculated for the electron energy upward the maximum potential distribution. The transmission coefficient, $\Gamma(x)$, calculated by the WKB approximation model for thermionic emission current calculation, is assumed to be one as shown in Fig.4.1.2, the $\Gamma(x)$ can be calculated if the electron energy over the maximum potential distribution. Fig4.4.3 shows the thermionic emission current density versus apply voltage by the unity, $\Gamma(x)$ equal to one, and unified transmission coefficient under the doping concentration of 10^{16} cm^{-3}. The transmission coefficient of unified method is smaller than the unity method under low doping concentration. As the $\Gamma(x)$ is an increasing function of forward bias and doping concentration. The simulation result of thermionic emission current at higher doping concentration is larger than unity simulation result as shown in Fig.4.4.4 and Fig.4.4.5. The opposite trend of forward and reserve bias is because the transmission coefficient strong depends on applied voltage.

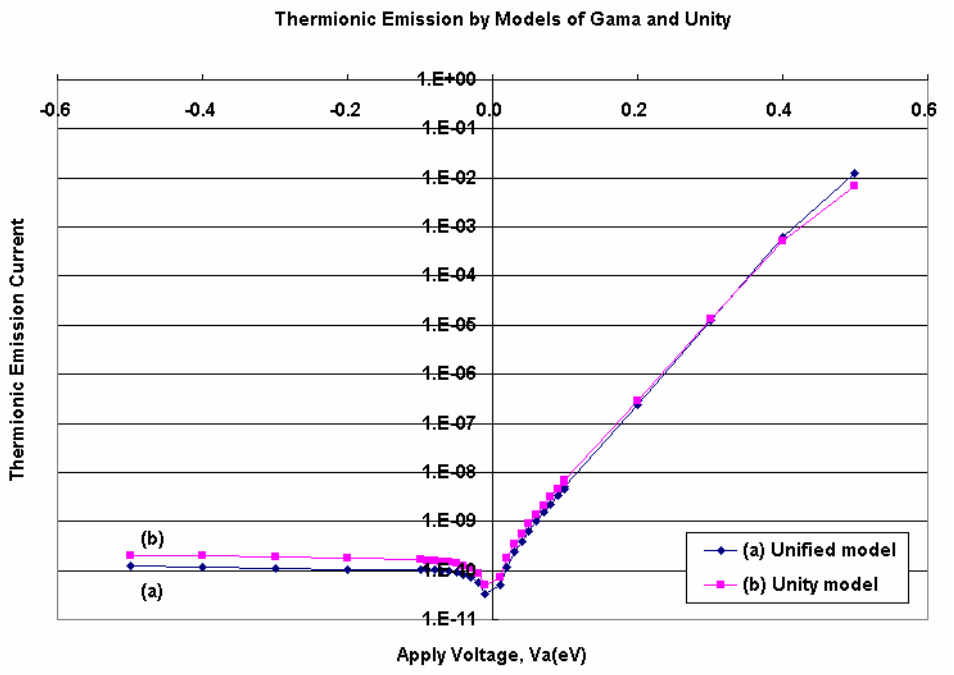

Fig. 4.4.3 Thermoinic-Emission current , J_{TE} vs apply voltage, for **a)** Unified and **b)** Unity Transmission Coefficient under conditions of barrier height 0.72eV and doping concentration Cd 10^{16} cm^{-3}

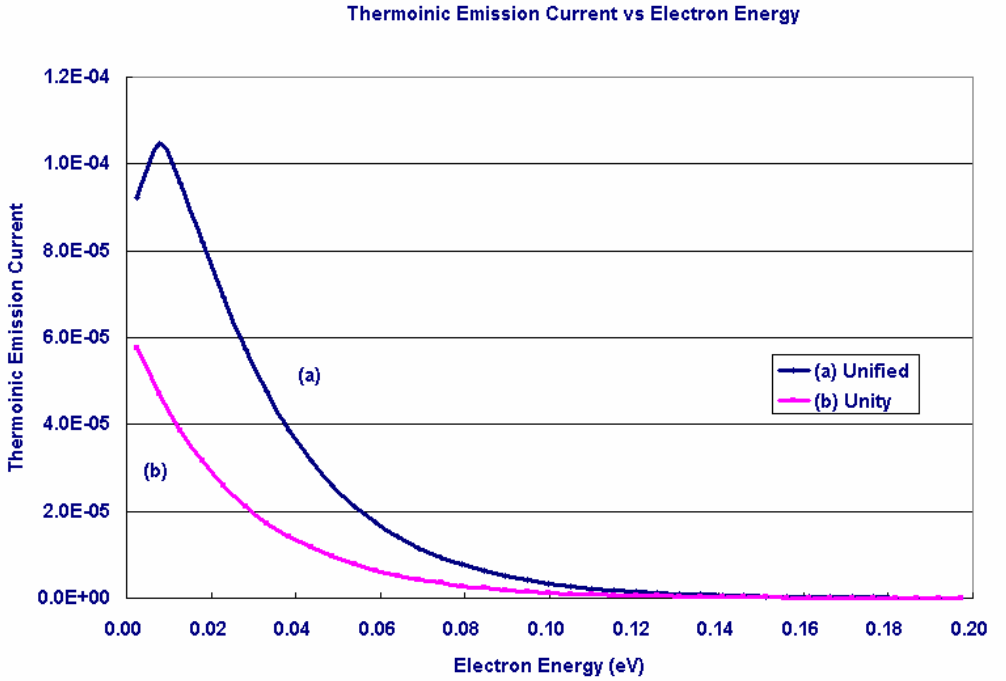

Fig. 4.4.4 Thermoinic-emission current vs electron energy, for a) Unified and b) Unity Transmission Coefficient under conditions of barrier height 0.72eV and apply voltage 0.5eV and doping concentration Cd 10^{20} cm^{-3}

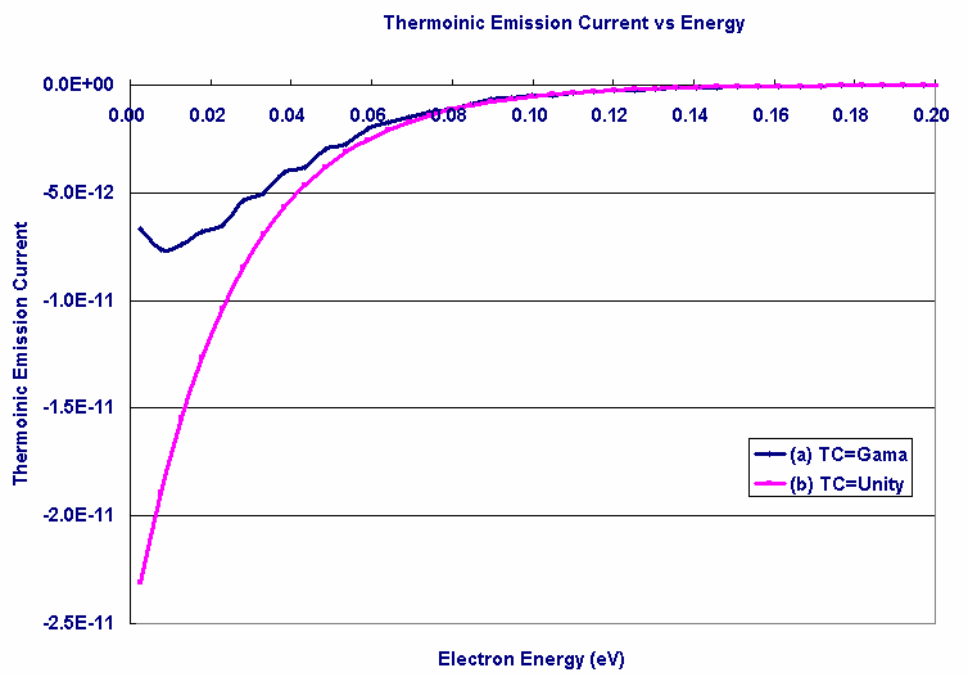

Fig. 4.4.5 Thermoinic-emission current vs electron energy, for **a)** unity and **b)** unified transmission coefficient under conditions of barrier height 0.72eV and apply voltage -0.5eV and doping concentration Cd 10^{20} cm^{-3}

Chapter 5 Conclusions

A unified simulation for the transmission of electrons through the metal-semiconductor contacts proved to be very useful for the calculation of tunneling current or thermionic current. The transmission coefficient for electrons with energy above or below the Schottky barrier can be calculated numerically using the Airy function or the exponential function. The tunneling processes have been self-consistently treated with all current transport in the semiconductor and more accurate results have been obtained for Schottky or Ohmic contact with a wide range of doping concentration. The degenerated model of transition probability can be applied to all range of impurity concentration while the non-degenerated model is suitable only to low doping semiconductors. Using the numerical model developed in this work, we can evaluate the performance of future nanometer devices such as Schottky S/D MOSFETs

Reference

[1] K, Matsuzawa, K, Uchida, and A. Nishiyama, " A Unified Simulation of Schottky and Ohmic Contacts," Electron Devices, IEEE Transactions, Vol. 47, p.103-108, 2000,

[2] S.F.Guo, "A Simple Model for Computer Simulation of Schottky-Barrier Diodes." Solid-State Electronics. Vol. 27, No. 6, p. 537-543, 1984

[3] R. Hattori and J. Shirafuji, "Numerical simulation of tunnel effect transistors employing internal field emission of Schottky barrier junction," *Jpn. J. Appl. Phys.*, vol. 33, p. 612, 1994.

[4] C.-K. Huang, W. E. Zhang, and C. H. Yang, "Two-dimensional numerical simulation of Schottky barrier MOSFET with channel length to 10nm," *IEEE Trans. Electron Devices* , vol. 45, p. 842, 1998.

[5] A. Schenk and S. Muller, "Analytical model of the metal-semiconductor contact for device simulation," *Simul. Semicond. Devices Processes*, vol. 5, p. 441, 1993.

[6] D. Schroeder and U. Witkowski, "Simulation of semiconductor devices with non-ideal metallic contacts," *IEEE Trans. Electron Devices* , vol. 44, p. 679, 1997.

[7] I. MeiKei, P.M. Solomon, S.E. Laux, H.-S.P. Wong, and D. Chidambarrao, "Comparison of Raised and Schottky Source/Drain MOSFETs Using a Novel Tunneling Contact Model." IEDM '98 Technical Digest., International, p.733–736, 1998

[8] J.V. Houdt, and K.D. Mayer, "A model for tunneling current in multi-layer tunnel dielectrics.", Solid-State Electronics, Vol. 47, p.1045-1053, 2003

[9] K.F. Brennan and C.J. Summers, "Theory of resonant tunneling in the variably spaced multiquantum well structure: An Airy function approach", J. Appl. Phys. Vol.61, No.2, Jan., 1987

[10] R.Tsu, and L.Esaki, "Tunneling in a finite superlattice.", Appl. Phys. Lett. Vol. 22,

No. 11, 1973

[11] S.Vatannin and G.Gildenblat, "Airy Functions Implementation of the Transfer-Matrix Method for Resonant Tunneling in Variably Spaced Finite Superlattices", IEEE Journal of Quantum Electronics, Vol. 32, No. 6, June 1996

[12] S.M. Sze, Physics of Semiconductor Devices, 2nd Edition, Central Book Company, Taiwan, 1983

[13] J. Cai, and C-T. Sah, "Gate tunneling in ultrathin oxide metal-oxide-silcon transistors", J. Appl. Phys., Vol.89, No.4, p.2272-2285, 2001

[14] L. Register, E.Rosenbaum, and K. Yang, "Analytic model for direct tunneling current in polycrystalline silicon-gate metal-oxide-semiconductor devices.", Appl. Phys. Lett., Vol. 74, No. 3, p.457-459,1999

[15] Y-S. Lou, and C-Y. Wu, "A Self-Consistent Characterization Methodology for Schottky-Barrier Diodes and Ohmic Contacts.", IEEE Transactions on Electron Device, Vol.41, No.4, 1994

[16] K. Shenai and R.W. Dutton, "Current Transport Mechanisms in Atomically Abrupt Metal-Semiconductor Interfaces", IEEE Transactions on Electron Device, Vol.35, No.4, 1988

Appendix

Appendix A
Algorithm for Airy Function (Bessel Function)

The Airy function of the first kind $Ai(x)$ can be defined to be

$$Ai(x)=\frac{1}{p}\int_0^\infty \cos\left(xt+\frac{1}{3}t^3\right)dt \tag{99}$$

It also can be expressed in terms of Bessel function of the first kind, $I_v(x)$

$$Ai(x)=\frac{1}{3}\sqrt{x}\left[I_{-1/3}\left(\frac{2}{3}x^{3/2}\right)-I_{1/3}\left(\frac{2}{3}x^{3/2}\right)\right] \tag{100}$$

Where the Airy function of second kind $Bi(x)$ is defined as

$$Bi(x)=\frac{1}{p}\int_0^\infty \exp\left(xt-\frac{1}{3}t^3\right)dt+\frac{1}{p}\int_0^\infty \sin\left(xt+\frac{1}{3}t^3\right)dt \tag{101}$$

Again, expressed by the Bessel functions of the second kind, $I_v(x)$, and Bessel functions of first kind, $J_v(x)$

$$Bi(x)=\sqrt{\frac{x}{3}}\left[I_{-1/3}\left(\frac{2}{3}x^{3/2}\right)+I_{1/3}\left(\frac{2}{3}x^{3/2}\right)\right],\quad for\quad x>0 \tag{102}$$

$$Bi(x)=\sqrt{\frac{-x}{3}}\left[J_{-1/3}\left(\frac{2}{3}|x|^{3/2}\right)-J_{1/3}\left(\frac{2}{3}|x|^{3/2}\right)\right],\quad for\quad x<0 \tag{103}$$

Bessel Function

A function of $I_n(x)$ which is one of the solutions of the Modified Bessel differential equation and closely related to the Bessel function of the first kind $J_n(x)$, where n is integer. The relationship of $I_n(x)$ and $J_n(x)$ is as following

$$I_n(x)\equiv i^{-n}J_n(ix)=e^{-npi/2}J_n\left(xe^{ip/2}\right) \tag{104}$$

For a real number v, the function can be computed using

$$I_v(x)=\left(\frac{1}{2}x\right)^v\sum_0^\infty\frac{\left(\frac{1}{4}x^2\right)^k}{k!\Gamma(v+k+1)} \tag{105}$$

Where Γ represent the gamma function

In term of the integral form,

$$I_v(x)=\frac{1}{p}\int_0^p e^{x\cos q}\cos(vq)dq-\frac{\sin(vp)}{p}\int_0^q e^{-x\cosh t-vt}dt \tag{106}$$

A derivative of expressing higher order of modified Bessel Functions in term of $I_0(x)$ is

$$I_n(x)=T_n\left(\frac{d}{dx}\right)I_0(x) \tag{107}$$

Where $T_n(x)$ is a Chebyshev polynomial of the first kind

$$I_0(x)=\sum_0^\infty\frac{\left(\frac{1}{4}x^2\right)^k}{(k!)^2} \tag{108}$$

The integral form of Airy Function no matter $Ai(x)$ or $Bi(x)$ can not apply to all x value if the x is too larger. That will cause the underflow issue when we calculate the $Ai(x)$ or $Bi(x)$. By using the Bessel can avoid the underflow issue which can apply to all x value and more accurate calculated results of the solution of Airy Function, $Ai(x)$ and $Bi(x)$

Appendix B

Normalization Factors

There is one important skill used in the program to simplify the calculation rout in the program. This can help to do convenient calculation in the derivation and numerical calculation. All quantities are normalized to dimensionless from the appropriate constants. The concept is described as following

Description	Symbol	Value	Unit
Electron charge	q	1.60218×10^{-19}	Coulomb
Electron rest mass	m0	0.91095×10^{-30}	Kg
Reduced Planck constant	hb	1.05458×10^{-34}	J-s
Permittivity of free space	e0	8.85418×10^{-14}	F/cm
Boltzmann constant	kb	1.38066×10^{-23}	J/K

Base on the Poisson of Eq.(56), can be written as

$$\frac{e_{Si}}{q^2 Nc}\frac{d^2 y}{dx^2} = \frac{p - n + Np}{Nc}, \tag{109}$$

to make the y dimensionless, the unit of x which is debye length LD can be written as

$$LD = \sqrt{\frac{q^2 Nc}{e_{Si} kt}} = \sqrt{\frac{qNc}{e_{Si} vkt}} \tag{110}$$

, where $$vkt = \frac{kt}{q} \tag{111}$$

$$tdi = \frac{LD}{vt}$$

$$hdi = q * Nc * vt \tag{112}$$

All the related normalization factors are listed on table B.1

Table B.1

Description	Symbol	Normalization Formula	Unit
⊕ Permittivity of silicon	esi	$11.9 * e0$	F/cm
⊕ Density of state effective mass of electrons in silicon	me	$me = (0.98 * 0.19^2)^{(1/3)} * m0$	
⊕ Thermal voltage	vkt	$vkt = kb * temp / q$	volt
⊕ Thermal velocity of free carrier	vt	$vt = 100\sqrt{(kb * temp)/(2 * me * Pi)}$	
⊕ Effective density of state in conduction band	Nc	$Nc = 2.8 * 10^{19} * (temp/300)^{1.5}$	#/cm^3
⊕ Debye length	LD	$LD = \sqrt{(esi * vkt)/(q * Nc)}$ $LDm = LD/100$ $LDnm = LD * 10^7$	cm m nm
⊕ Current density normalization factor	hdi	$hdi = q * Nc * vt$	amp/cm^2
⊕ time normalization factor	tdi	$tdi = LD / vt$	sec

+

Schrödinger Equation of Eq.(1)

Refer to chapter 3.2 which show the solution of Schrödinger equation in region I/II/III

$$y_1(x) = e^{ik_1 x} + \mathrm{Re}^{-ik_1 x} \quad , \; k_1 = \sqrt{\frac{2mE}{\hbar^2}} \tag{113}$$

$$y_2(x) = C_2^+ e^{k_2 x} + C_2^- e^{-k_2 x} \quad , \; k_2 = \sqrt{\frac{2m(V_2 - E)}{\hbar^2}} \tag{114}$$

$$y_3(x) = Te^{ik_3 x} \quad , \; k_3 = \sqrt{\frac{2m_1(E - V_3)}{\hbar^2}} \tag{115}$$

To sim plify the calculation, the K1/K2/K3 in program are represented in the following table which is easier for program writing.

Table B.2

Description	Symbol	Normalization Formula	Unit
⌖ simplified K1	$k1$	$k1 = LDm * \sqrt{(2 * m0 * kb * temp)/hb}$	
⌖ simplified K2	$k2$	$k2 = LDm * \sqrt[1/3]{(2 * me * kb * temp)/(LDm * hb^2)}$	
⌖ simplified K3	$k3$	$k3 = LDm * \sqrt{(2 * me * kb * temp)/hb}$